Direct comparison of the tsunami-generated magnetic field with sea level change for the 2009 Samoa and 2010 Chile tsunamis

Zhiheng Lin[1], Hiroaki Toh[2], and Takuto Minami[3]

[1]Division of Earth and Planetary Sciences, Graduate School of Science, Kyoto University

[2]Data Analysis Center for Geomagnetism and Space Magnetism, Graduate School of Science, Kyoto University

[3]Department of Planetology, Faculty of Science, Kobe University

Corresponding author: Z. Lin (lin.zhiheng.58x@st.kyoto-u.ac.jp)

Key Points:

- Direct comparison of the observed tsunami magnetic field with tsunami sea level change for the 2009 Samoa and 2010 Chile tsunamis.

- 3-D time domain simulation of both tsunami sea level change and magnetic field for the 2009 Samoa and 2010 Chile earthquake tsunamis.

- Estimation of the tsunami wave height by the tsunami-generated magnetic field.

Plain Language Summary

In the previous studies, researchers claimed that the tsunami-generated magnetic field arrives earlier than the tsunami sea level change based on analytical solutions and numerical simulations. In this paper, we used the world's first simultaneous data of sea level change and magnetic field in the 2009 Samoa and 2010 Chile tsunamis to study the relation between these two physical quantities. We found that the vertical component of tsunami magnetic field arrives earlier than the sea level change. Moreover, the horizontal component of tsunami magnetic field arrives even earlier than the vertical component. The tsunami magnetic field was also revealed that it can be used to estimate the tsunami wave height very accurately. We investigated the observed tsunami magnetic field by our 3-D time-domain simulation. However, the currently existing tsunami source models were unable to reproduce the observation in our research area. We confirmed that a better source model can improve the simulation. It follows that our high precision tsunami wave height data converted from the magnetic field should be used to construct a better tsunami source model.

Abstract

The tsunami-generated magnetic field on seafloor was found to be a powerful tool for the tsunami early warning. Using the magnetic field, it is possible to detect the propagation of tsunamis and to estimate their wave height prior to their actual arrivals because it arrives earlier than the tsunami sea level change and very sensitive to it. However, these correlations have never been studied by the direct comparison between the observed tsunami magnetic field and sea level change. This study aims at the correlation between the tsunami magnetic field and sea level change using the observed data and the three-dimensional (3-D) simulation of the 2009 Samoa and 2010 Chile earthquake tsunamis. The comparison of the observed tsunami magnetic field and observed sea level change illustrated that the vertical component of tsunami magnetic field, Bz, has a phase lead to the sea level change. Combined with the 3-D simulation results, the initial rise in observed tsunami Bh which also arrives earlier than the tsunami sea level change was confirmed. We further examined the precision of conversion of the tsunami magnetic field to the sea level change. The results suggest that the converted tsunami sea levels have as high precision as the differential pressure gauge data. However, our simulation was unable to reproduce the observation well, because of the inaccurate tsunami source models. It, therefore, is necessary that the very precise sea level changes converted from the observed tsunami magnetic field should be used in constructing new tsunami source models.

1 Introduction

Faraday's law of induction tells us that a conductor cutting a background magnetic field generates an electric field. The tsunami-generated magnetic field (we call it the 'tsunami magnetic field' hereafter) is a magnetic field generated by the tsunami's electromotive force of the moving conductive seawater cutting the geomagnetic main field. The tsunami magnetic field was found to arrive earlier than the tsunami sea level change (e.g., Toh et al., 2011), which can be exploited to detect tsunami events (Minami and Toh, 2013; Zhang et al., 2014; Schnepf et al. 2016; Minami et al., 2017) and estimate their wave height (Tyler, 2005; Sugioka et al., 2014; Minami et al., 2015; 2021) for the global tsunami early warning system such as DART (Deep-ocean Assessment and Reporting of Tsunamis; Bernard et al., 2011). Furthermore, it can be used to estimate the source mechanism of the tsunamigenic earthquake in concern (Kawashima and Toh, 2016). To those ends, the early arrival and sensitivity of tsunami magnetic fields w.r.t. the sea level change need further study.

The signal of tsunami in the vertical component of the magnetic field, Bz, may arrive earlier than the sea level change, which has been predicted by analytical solutions (Tyler, 2005; Minami et al., 2015; 2021) and numerical simulation (Minami et al., 2015). This feature means that using tsunami Bz, we can detect tsunamis before their actual arrival. The leading phase of tsunami Bz is between the 0º to 90º, which mainly depends on the ocean depth (Minami et al., 2015). In their study, the tsunami-generated magnetic field was classified into three categories according to the phase lead angle of tsunami Bz: The self-induction dominant case appears in deep waters with phase leads of 0º~20º. Also, 20º~70º for the intermediate case and 70º~90º for the diffusion dominant case that appears in shallow waters. However, in studies of the 2011 Tohoku event (Zhang et al., 2014, Minami et al., 2017), the phase lead of tsunami Bz was not identified clearly by comparison of the simulated sea level change with the observed magnetic field. Hence, there remains a need to confirm the phase lead of tsunami Bz by simultaneous observation of both tsunami sea level change and tsunami Bz.

There also exists a tsunami magnetic signal in the horizontal component, Bh, which arrives even earlier than tsunami Bz (Minami and Toh, 2013; Minami et al., 2015). The signal was coined an "initial rise" by them and is the very first tsunami signal. The initial rise in tsunami Bh was first recognized by the 2-D tsunami magnetic simulation of the 2011 Tohoku tsunami by Minami and Toh (2013) and confirmed by the observation and 3-D simulation of the 2011 Tohoku tsunami (Zhang et al., 2014; Minami et al., 2017). However, the initial rise was not recognized in other tsunami events such as the 2006 and 2007 Kuril earthquake tsunamis (Toh et al., 2011). Because the initial rise is promising for tsunami early warning, it is necessary to examine its presence in more tsunami events.

The tsunami magnetic components Bz and Bh can be converted into the tsunami sea level change (and vice versa) using the frequency-domain 2-D analytical solution of tsunami magnetic fields for linear dispersive tsunamis (Minami et al., 2021). The conversion allows us to estimate the tsunami wave height before its arrival using the tsunami magnetic field. A simpler conversion equation between the tsunami Bz and sea level change based on the long wave approximation was reported by Tyler (2005). Minami et al. (2021) indicated that there is nearly a linear relation between the amplitude of tsunami Bz and sea level change in the tsunami frequency band. Moreover, the 2-D analytical solution for linear dispersive tsunamis provides a better conversion method to calculate the tsunami sea level change from both tsunami Bz and Bh (and vice versa). Unfortunately, the conversion has not yet been examined by direct observation

so far due to the lack of the simultaneous observation of both tsunami magnetic field and sea level change at the same site.

Numerical simulations of tsunami magnetic fields play an important role in search for the phase lead of Bz and the initial rise in Bh. However, most of the actual tsunami simulations were focused only on the 2011 Tohoku earthquake event (Minami and Toh, 2013; Zhang et al., 2014; Minami et al., 2017). Even though the simulated tsunami magnetic fields in those previous studies still have discrepancy from the observed magnetic field, no assessment on the validity of the used tsunami velocity field has been given due to the lack of the simultaneous observation of both tsunami magnetic field and sea level change again.

In this paper, we deal with the tsunami magnetic field of the 2009 Samoa and 2010 Chile tsunamis observed on the French Polynesian seafloor in the south Pacific Ocean (TIARES Project: Suetsugu et al., 2012). What is most unique to this dataset is that it contains a simultaneous observation of both tsunami magnetic field and sea level change at Site SOC8. We will address the following questions in this paper:

1. Are the phase lead of the tsunami Bz and the initial rise in tsunami Bh really present in the observation?

2. Does the conversion between the tsunami sea level change and magnetic field have enough precision?

3. What is the main error source in the simulation of tsunami magnetic fields?

For those purposes, we first introduce the observation of the 2009 Samoa and 2010 Chile tsunamis in Section 2. In Section 3, we will make a direct comparison of the observed tsunami sea level with the observed tsunami magnetic field to study the phase lead of tsunami Bz and the initial rise in Bh appeared in the observation. We will also compare the tsunami sea level change converted from the observed magnetic field with the observation to examine precision of the tsunami wave height estimated by the tsunami magnetic field. In Section 4, we will show the result of the 3-D time domain simulation of the tsunami magnetic field for both events. Combining the observation and the simulation results, the phase lead of Bz and the initial rise will be further examined. Finally, all the results will be discussed and concluded in terms of the three questions given above in the last section.

2 Observed data

The observed tsunami magnetic and pressure data of the 2009 Samoa and 2010 Chile earthquakes were used in this study. Those data were acquired in a geophysical observation campaign, named TIARES (Tomographic Investigation by seafloor Array Experiment; Suetsugu et al., 2012), on the French Polynesian seafloor in the South Pacific Ocean from February 2009 through November 2010 as shown in Fig. 1. As listed in Table 1, this experiment deployed an observation array consisting of 9 Ocean Bottom ElectroMagnetometers (OBEMs) and a Differential Pressure Gauge (DPG) on the 4000~5000m deep seafloor for investigating the electrical conductivity structures of the mantle beneath the Society hotspot in addition to ocean bottom seismometers for tomographic purposes. Three-component magnetic field data were recorded by the OBEMs: Bx in the geographical north direction, By in the geographical east direction and Bz in the downward direction with a 1-minute sampling rate. The pressure data was observed by the DPG at Site SOC8 with a 1-second sampling rate.

The observation array in the TIARES area captured the signals of the tsunami-generated magnetic field as well as the ocean bottom pressure change when the earthquake tsunamis passed over the TIARES area, on the 29th of September in 2009 and the 27th of February in 2010 at the times of the Samoa earthquake of M_w 8.1 and the Chile earthquake of M_w 8.8 as listed in Table 2. The geomagnetic activities were small on those dates, whose Kp-indices were 0 and 1- on the days of the Samoa and Chile tsunami events, respectively (Matzka et al., 2021). As a result, the tsunami-generated magnetic fields were detected clearly in the observed time-series, although the observation area was very far from both epicenters (~3000 km for the 2009 Samoa earthquake and ~7000 km for the 2010 Chile earthquake).
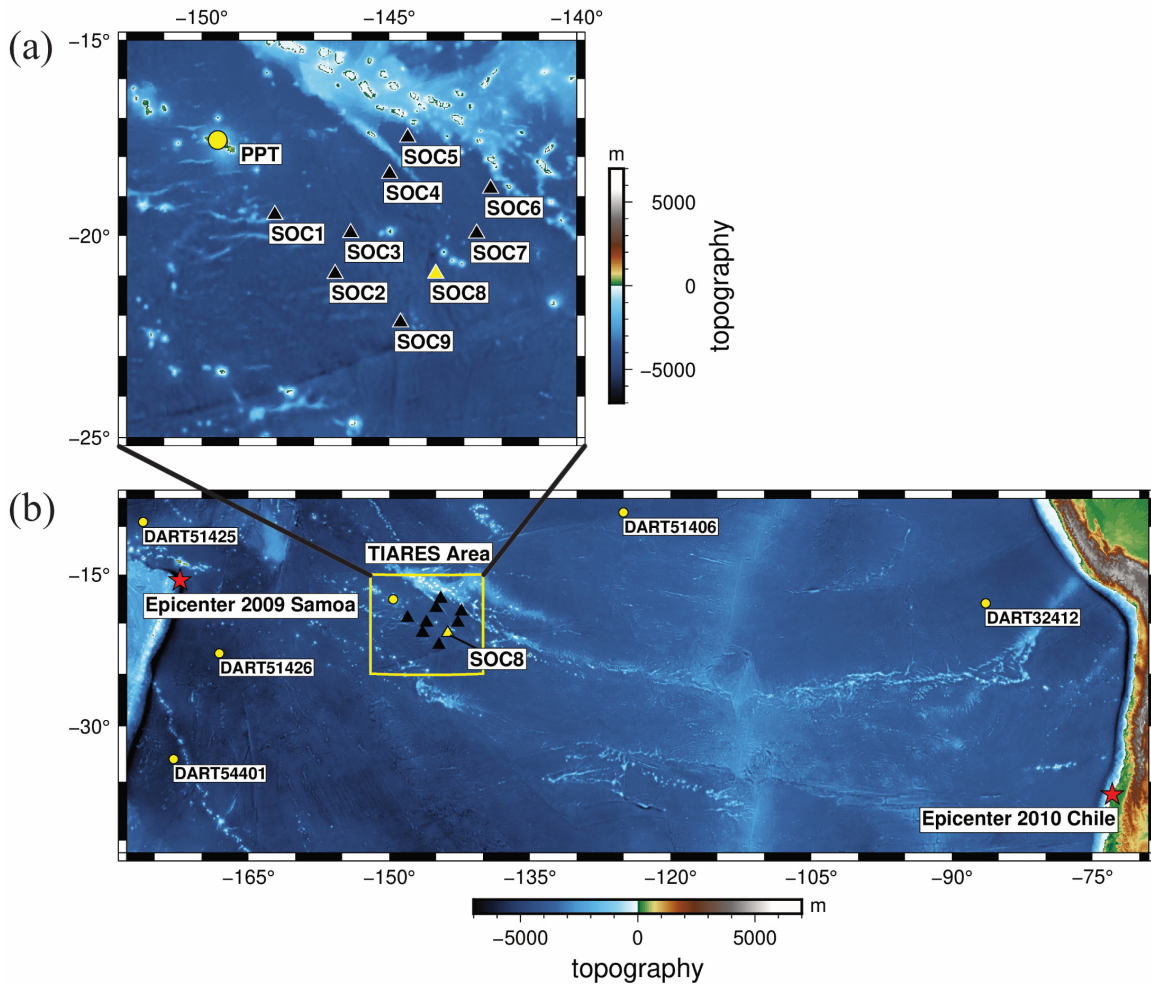

Figure 1. (a) A map showing the topography/bathymetry around the TIARES area and the location of SOC1-9 (triangles) and Pamatai (PPT) geomagnetic observatory (yellow circle) on Tahiti Island. (b) A map showing the location of the epicenters of the 2009 Samoa and 2010 Chile earthquakes (red stars), the DART stations (yellow circles) and the TIARES area (the yellow rectangle). These maps were drawn by Generic Mapping Tools (GMT) v.6.1.1 (Wessel et al., 2019; https://www.generic-mapping-tools.org) based on the 30 arc second global relief (SRTM15+V2.1, Tozer et al., 2019).

Table 1. Locations, observed physical quantities and observation periods at SOC1 through 9

Station Name	Latitude(°)	Longitude(°)	Depth (m)	Observed Signals	Observed Period
SOC1	19.4682S	148.0498W	4427	EM	2 March 2009 to 23 November 2010
SOC2	20.9561S	146.4423W	4772	EM	2 March 2009 to 15 October 2010
SOC3	19.9286S	146.026W	4656	EM	2 March 2009 to 18 March 2010
SOC4	18.4281S	144.9878W	4478	EM	2 March 2009 to 25 July 2010
SOC5	17.5012S	144.5069W	4049	EM	2 March 2009 to 3 June 2010
SOC6	18.8055S	142.2961W	4508	EM	2 March 2009 to 19 July 2010
SOC7	19.9405S	142.6682W	4490	EM	2 March 2009 to 27 July 2010
SOC8	20.9548S	143.757W	4806	**EM and Pressure**	2 March 2009 to 10 October 2010
SOC9	22.1675S	144.6965W	4540	EM	2 March 2009 to 29 June 2010

Table 2. Locations and distances from the epicenters of the 2009 Samoa and 2010 Chile earthquakes to the TIARES area, the estimated times of tsunami arrival at the TIARES area and the Kp-indices at the time of each tsunami event.

Event	UTC Time	Latitude (°)	Longitude (°)	Depth (km)	Magnitude (Mw)	Distance to TIARES area (km)	ETAs to TIARES area	Kp-index
Samoa	2009-09-29 17:48:10	15.6163 S	172.3019 W	16.86	8.10	~3000	2009-09-29 21:10 ~ 22:10	0
Chile	2010-02-27 06:34:23	36.2080 S	72.963 W	31.64	8.80	~7000	2010-02-27 16:40 ~ 17:15	1-

In this study, we extracted the tsunami signals from the observed magnetic and pressure data and collated the two different physical quantities, details of which can be seen in the Supporting Information. The observed pressure data were processed by the following three steps: First, the raw DPG data were deconvoluted to transform them into the real pressure variations [Pa] on the seafloor in which the deconvolution equation of Araki and Sugioka (2009) was used. Second, the pressure data thus restored were converted into the sea level change [m] with a constant of 100 Pa/cm. Finally, a band-pass filter was applied to the sea level changes to recover the wave height at the time of the tsunami events. The pass bands were 3~30-minute and 3~45-minute for the Samoa and Chile tsunamis, respectively, which were estimated by the prior wavelet analyses of the sea level changes at the time of the tsunamis passage. On the other hand, processing of the magnetic data was conducted in two steps: First, the same band-pass filter as the sea level changes was applied to the observed time series to extract the signals in the tsunami frequency band. Second, the transfer function method (Minami et al., 2017) was further applied to eliminate the geomagnetic fluctuations of external origin in signals of the tsunami frequency band, although the geomagnetic activities on the days of the tsunami events were small enough.

3 Observed tsunami magnetic field and sea level change

By the data processing described above, we succeeded in extracting the tsunami magnetic signal, (Bx, By, Bz), from the observed data. The horizontal magnetic components, Bx and By were further rotated to the direction of the tsunami propagation, N96.2ºE for the Samoa tsunami and N47.5ºW for the Chile tsunami in order to yield the horizontal tsunami magnetic signal, Bh. Here we compare the tsunami Bz and Bh time-series in Fig. 2.
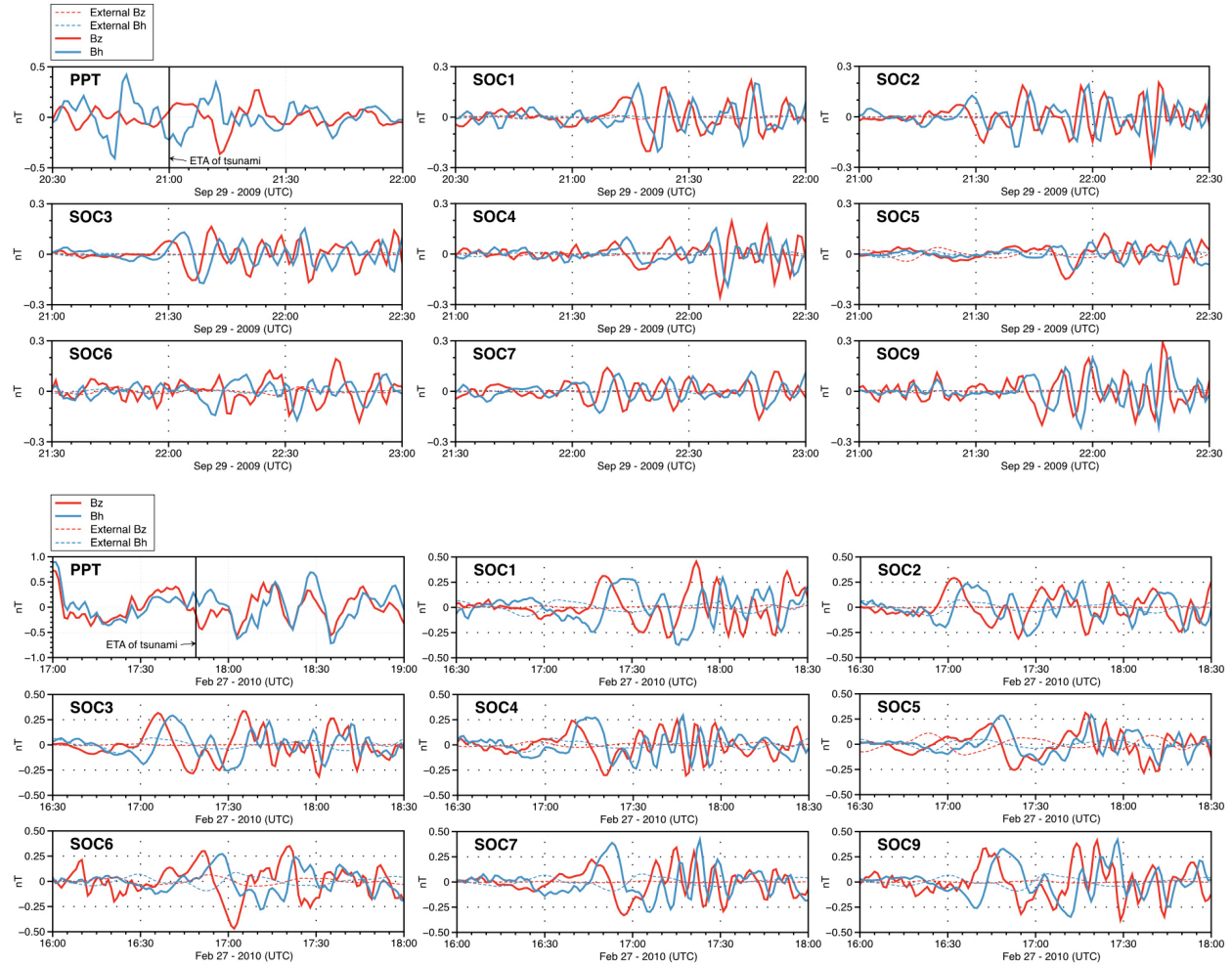

Figure 2. Comparison of the tsunami Bz and Bh for the 2009 Samoa event (upper penal) and 2010 Chile event (lower penal). The magnetic field components have passed through a 3~30-minute and 3~45-minute band-pass filter for the Samoa and Chile tsunamis respectively, and the external field (dashed lines) has been subtracted as well. It is evident that the tsunami Bz (red lines) always leads Bh (blue lines) as large as ~90º in phase at the SOC stations on the seafloor.

The tsunami magnetic fields of the 2009 Samoa and 2010 Chile tsunamis are clearly seen in Fig. 2. One of the main features of the tsunami magnetic field on the seafloor is that the tsunami Bz phase leads Bh by ~90º, which has also been confirmed by the observation of the 2006 and 2007 Kuril earthquake tsunamis (Toh et al., 2011) and the 2011 Tohoku tsunami

(Minami et al., 2017). The amplitudes are about 0.2 nT and 0.3 nT for the 2009 Samoa and 2010 Chile tsunamis, respectively. On the other hand, when the tsunami passed by (black solid vertical lines in Fig. 2), the tsunami magnetic signals at Pamatai (PPT), the closest land observatory to the TIARES area, were not visible even after the same band-pass filtering as the SOCs data. It may be because the land station is exposed to large magnetic noises of external origin without a thick cover of conductive seawater compared with the seafloor stations.

The data at the SOC8 station is very unique in the sense that it is the world's first simultaneous data of both ocean bottom pressure and magnetic field (Suetsugu et al., 2012). This enabled us to study the following two topics:

1. The phase lead of tsunami Bz and the initial rise in Bh w.r.t. the tsunami sea level change.

2. The conversion of tsunami magnetic field to tsunami sea level change (and vice versa).

The former can help us to investigate the tsunami early warning ability of the tsunami magnetic field. Moreover, the conversion of the tsunami magnetic field to the tsunami sea level allows us to examine the validity of our procedure to extract the tsunami magnetic field.
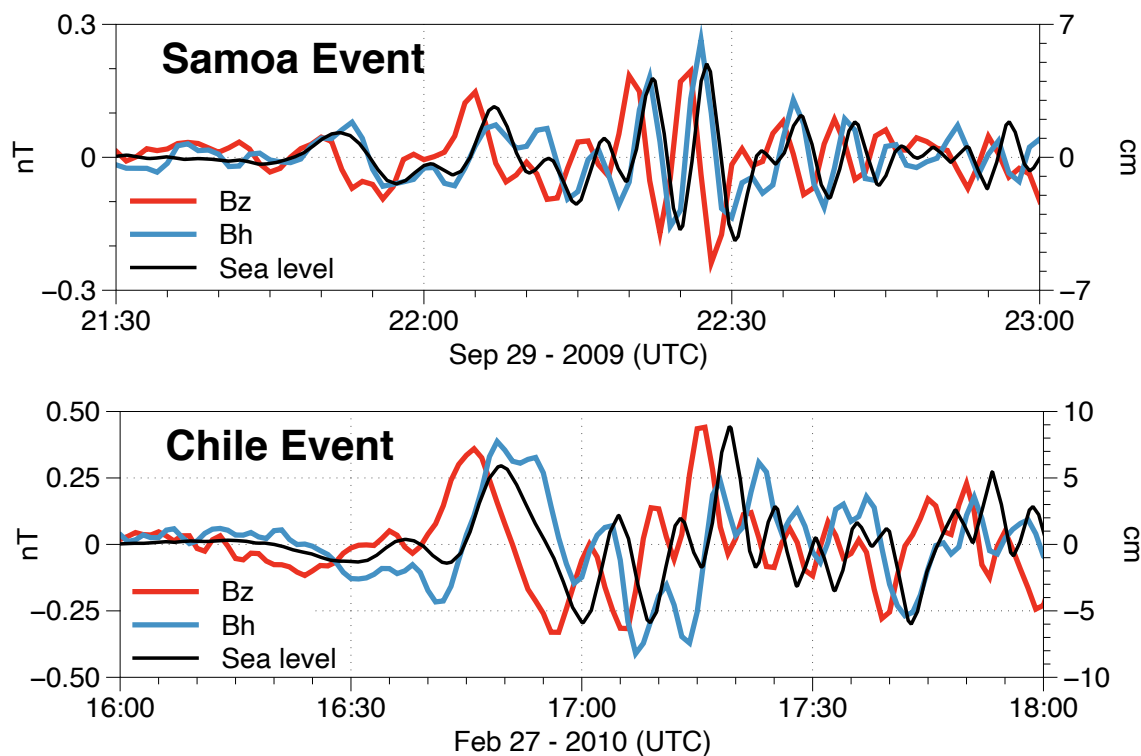

Figure 3. Comparison of the observed magnetic field with the sea level change at SOC8. The upper penal is for the 2009 Samoa tsunami, and the lower is for the 2010 Chile tsunami. The sea level changes were deconvoluted from the observed pressure data using the response equation of Araki and Sugioka (2009). The external field has been subtracted from the observed magnetic field components as before. The observed sea level changes and magnetic signals of the 2009 Samoa and 2010 Chile tsunamis have passed through the 3~30-minute and 3~45-minute band-pass filters, respectively. This comparison clearly shows the phase lead of tsunami Bz w.r.t. the observed sea level changes.

The phase lead of tsunami Bz and the initial rise in Bh have been simulated by several previous studies (Minami and Toh, 2013; Minami et al., 2015; 2017). However, they have never been verified by comparison of observed tsunami sea level changes with observed tsunami magnetic fields, which has been done for the first time by this study as shown in Fig. 3.

As can be seen from the direct comparison of the observed sea level change and magnetic field, the observed tsunami Bz (red lines) arrived earlier than the sea level change (black lines), while Bh (blue lines) were delayed compared with tsunami Bz. We calculated the phase differences between the magnetic components and the sea level change for the main periods of both events and illustrated them in Fig. 4. As shown in that figure, the longer the periods of magnetic variations are, the larger the time difference between the sea level change becomes linearly, which implies we will have flat curves when convert the time differences into phases. The phase differences become flat as expected as shown in the right panel of Fig. 4. Bz components arrived earlier than the sea level change with phase leads of about $10° \sim 40°$, while Bh components arrived later that the sea level change with phase lags of about $60° \sim 90°$. These phase differences agree well with prediction of the 2-D analytical solution by Minami et al. (2021) and fall in the "Self-induction dominant case" and "Intermediate case" of Minami et al. (2015). It means that the tsunami magnetic field generated by self-induction is strong here.
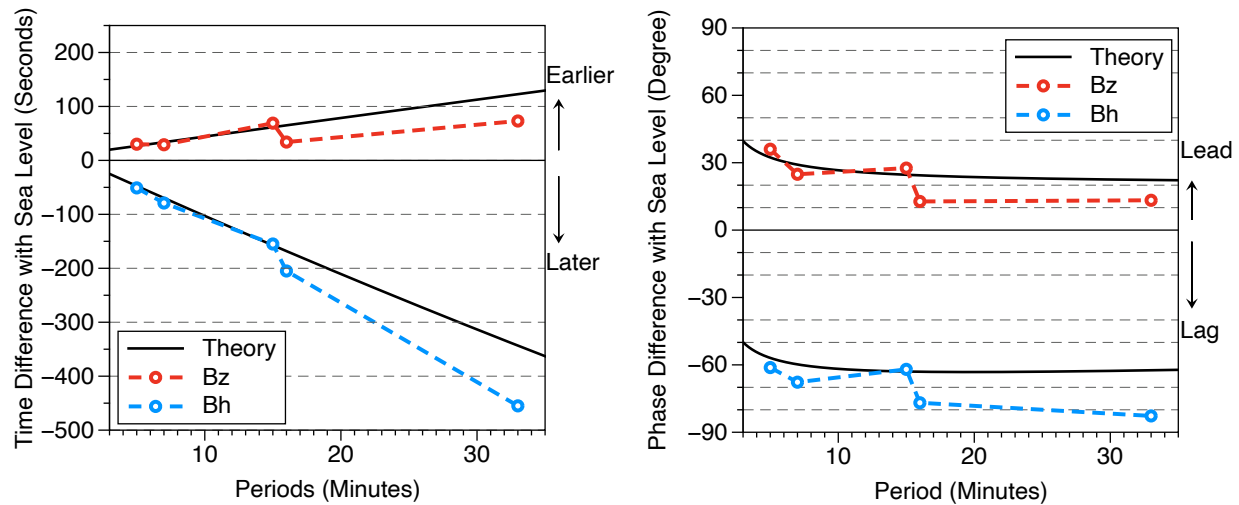

Figure 4. The time (left) and phase angle (right) differences of the tsunami Bz and Bh w.r.t. the sea level change within the main periods of the 2009 Samoa and 2010 Chile tsunamis at SOC8. The time and phase differences were calculated by measuring the difference between the wavelet form of the observed tsunami sea level change and magnetic components within the main period bands (5 and 16 minutes for Samoa, and 7, 15 and 33 minutes for Chile tsunamis; see Supporting Information). The black solid lines are the theoretical values with the 0.01 S/m seafloor conductivity using Minami et al. (2021). The observed time and phase differences are in line with the analytical solutions.

The initial rise in tsunami Bh was first proposed by Minami and Toh (2013). However, it is hard to recognize in both of the observed horizontal magnetic fields shown in the Fig. 3. In the 2009 Samoa tsunami, we are unable to recognize the initial rise in tsunami Bh. It seems that the

initial rise is the same level as the background noise. In the 2010 Chile tsunami, we cannot confirm whether the negative peak in Bh is the initial rise or not. One way to explain that is combining the observation with the simulation result which will be shown in next section.

To evaluate the precision of converting the tsunami magnetic field to the tsunami sea level change, the converted sea level changes from the Bz and Bh of SOC8 were compared with the actual sea level changes in top left penal of Fig. 5 for the 2009 Samoa and 2010 Chile tsunamis. The converted sea level changes of other SOCs are also shown in the figure. The tsunami sea level change can be estimated using the magnetic components Bz and Bh (Tyler, 2005; Sugioka et al., 2014; Minami et al., 2015; 2021). Here, we used the 2-D analytical solution by Minami et al. (2021) for linear dispersive waves with the 0.01 S/m seafloor conductivity to calculate the sea level changes from the observed Bz and Bh.
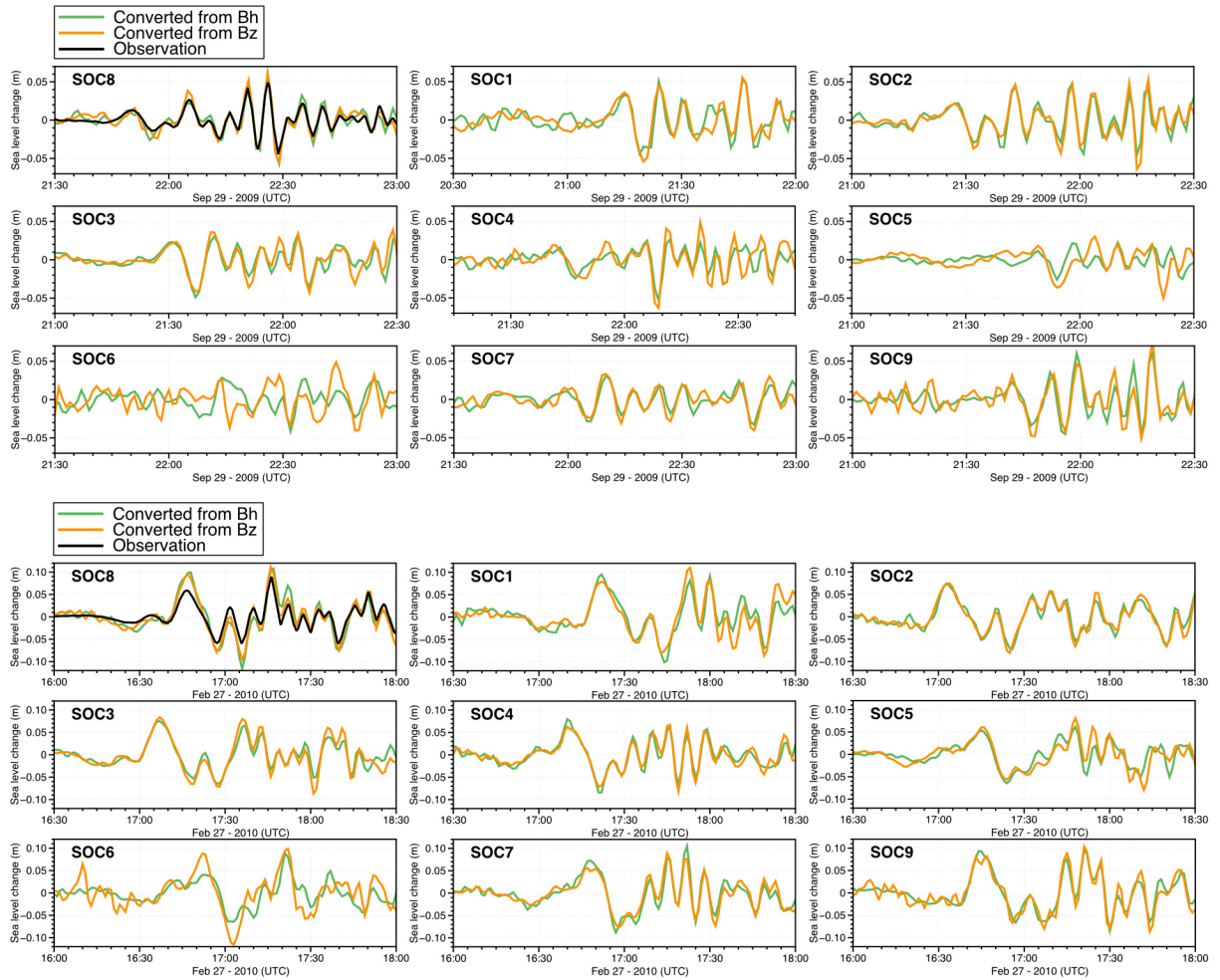

Figure 5. Comparison of the converted sea level changes from Bz and Bh. The upper nine panels are for the 2009 Samoa tsunami, and the lower nine are for the 2010 Chile tsunami. The observed sea level changes at SOC8 are also shown in the top left panel for each tsunami. The converted sea level changes were calculated by the 2-D analytical solution of tsunami magnetic field (Minami et al., 2021) using the filtered magnetic fields. The comparison shows the excellent agreement between the converted and the observed tsunami sea level changes at SOC8 and the consistency between these two converted sea level changes except for SOC6.

The comparison of the observed sea level change and the converted results of the Samoa tsunami at SOC8 shows the excellent agreement with each other. Also, the results at other SOCs show good agreement between these two converted sea level changes and their consistency. These results not only indicate that the tsunami magnetic signals were cleary extracted from the observed data by our data processing, but also mean that the tsunami Bz and Bh are very sensitive to the sea level change even for tsunamis smaller than 0.1m, in other words, we can estimate the sea level change by the tsunami magnetic field with high precision. Because the tsunami magnetic field arrives earlier then the tsunami itself, we can estimate the tsunami wave height before its arrival. However, in the results of the 2010 Chile tsunami at SOC8 still have discrepancy in amplitude between 16:40~17:30. It may be due to the higher 3-D effect of the 2010 Chile tsunami than the 2009 Samoa tsunami. In order to investigate the discrepancy further, 3-D tsunami kinetic/electromagnetic simulations will be introduced in the next section.

4 Simulation of tsunami magnetic fields for the 2009 Samoa and 2010 Chile events

The 3-D time domain tsunami magnetic simulation was conducted to explain the two issues in the observation: 1. The missing initial rise in the Samoa event. 2. The 3-D effect found by the conversion of the Chile tsunami magnetic field to the sea level changes. To those ends, the 3-D simulation results will be compared with the observation. On the other hand, the observed sea level change along with the magnetic field at SOC8 allows us to estimate the error of tsunami velocity and magnetic field calculation separately. Namely, we will discuss the main error source in the simulation of tsunami magnetic field.

The simulation of the tsunami magnetic field of the 2009 Samoa and 2010 Chile events over the TIARES area consisted of the following two steps: First, the tsunami velocity field in the TIARES area were simulated kinetically using an open-source software, and then the tsunami magnetic field were calculated using the velocity field thus simulated. Finally, the simulated tsunami magnetic fields were compared with the observed magnetic fields at all SOC stations in the TIARES area.

4.1 Simulation of the tsunami velocity field

The TIARES area is considerably distant from the two epicenters as listed in Table 2 and the two tsunamis contained multiple frequencies (Schnepf et al. 2016), which means that the dispersion of the tsunamis should be considered. In this study, an open-source tsunami simulation code, JAGURS, by Baba et al. (2017) was used for calculation of particle motions of the tsunamis in concern because it can account for the effects of Boussinesq dispersion as well as elastic loading.

JAGURS simulates the velocity field based on earthquake fault models that are normally inverted from the seismic and tsunami data. Proper fault models are indispensable for decent tsunami velocity simulations. Several source models reported by previous research have been considered in this study. Our guiding principle of the fault model selection was that it can fit the sea level changes around the TIARES area most.

For the 2009 Samoa tsunami, we used the 'Mega 1' fault model of Fritz et al. (2011), which is a single normal fault model and can explain the observed sea level of the DART stations near the TIARES area (see Fig. 11 of Fritz et al., 2011). As for the 2010 Chile tsunami,

we used the 'all DART only' fault model of Yoshimoto et al. (2016), because it is a multiple-fault model obtained by the inversion of the tsunami data at 26 DART stations over the Pacific. These fault models show the best fit to the tsunami sea level around the TIARES area among the existing source models, although they did not include the sea level change data at SOC8.
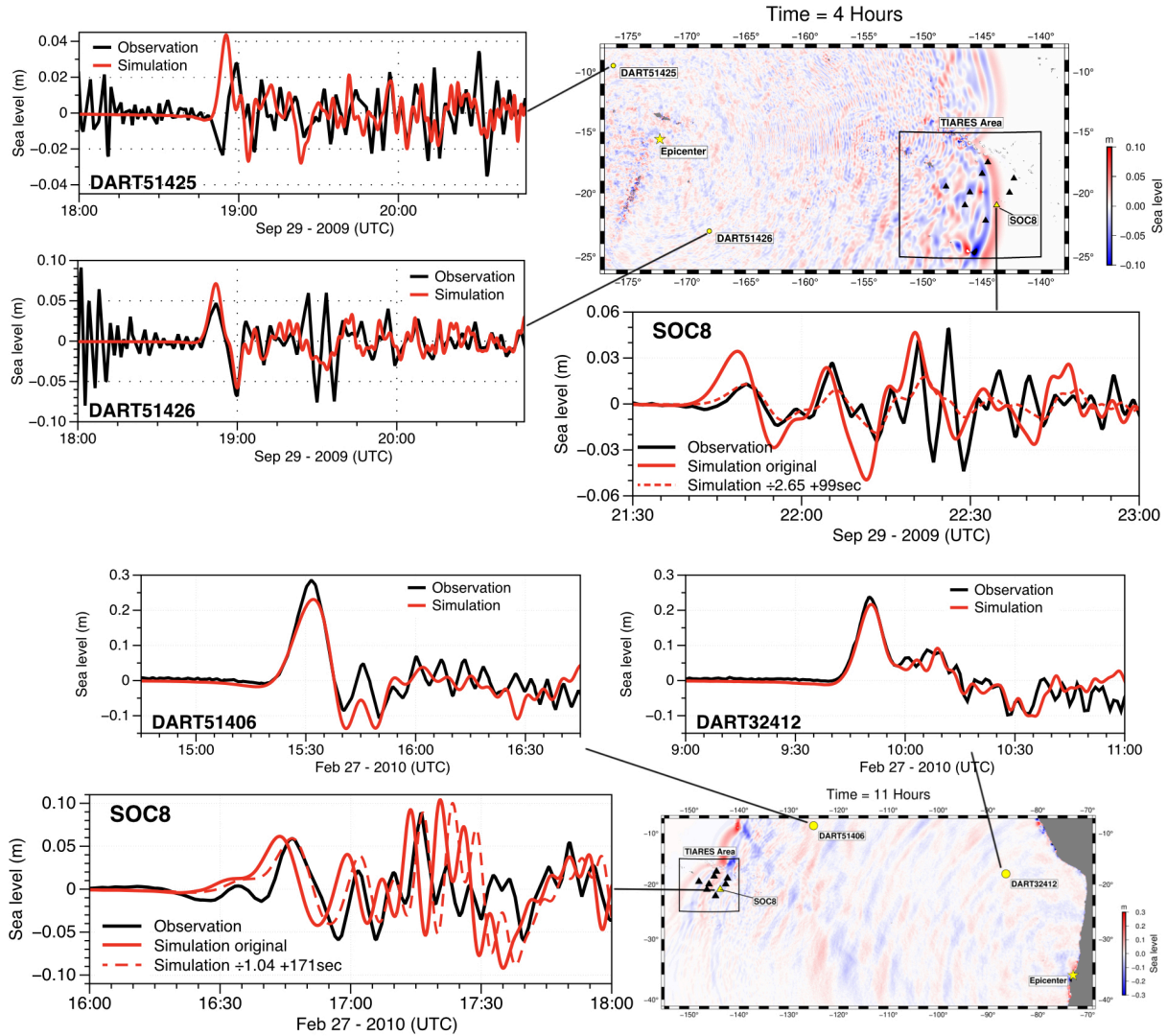

Figure 6. The upper 4 panels are the area of the 2009 Samoa tsunami velocity field simulation (upper right) and the comparison of the simulated and observed sea levels for DART51425, 51426 and SOC8. The lower 4 panels are the area of the 2010 Chile tsunami velocity field simulation (lower right) and the comparison of the simulated and the observed sea levels for DART32412, 51406 and SOC8. The sea levels were calculated by JAGURS, while the DART data were downloaded from the NOAA website (https://www.ngdc.noaa.gov/hazard/dart/2009 samoa_dart.html; https://www.ngdc.noaa.gov/hazard/dart/2010chile_dart.html). Observed sea levels were from the DPG at SOC8 (Suetsugu et al., 2012). In the upper penal of Samoa tsunami, the simulation explains the observed sea level well at the DART51426 and agree fairly well at SOC8 if the original observation is divided by 2.65 and delayed by 99s (the red dashed line in the lower right). While the Chile tsunami in lower penal, the simulation results explain well the observed sea level at both DART stations, while the data at SOC8 still needs further modification that is divided by 1.04 and delayed by 171s (the red dashed line in the lower left).

Properties of the velocity field simulation by JAGURS for the 2009 Samoa and 2010 Chile tsunamis are shown in Table S1 in Supporting Information. The velocity fields of the tsunamis were simulated from the epicenters through the TIARES area for time spans of 7 hours for the Samoa event and 14 hours for the Chile event. In order to examine our simulation results, the DART stations of 51425 and 51426 were included in the simulation in the case of the 2009 Samoa tsunami, while the DART stations of 32412 and 51406 were incorporated in the 2010 Chile tsunami simulation. Comparison of the simulated and observed sea levels at the DART stations and Site SOC8 in the TIARES area for both events is shown in Fig. 6.

Figure 6 shows that our simulation at the DART stations is in line with the result of the previous works. For the Samoa tsunami, the simulated sea level at DART 51425 and 51426 were successfully reproduced as those in Fritz et al. (2011). However, this fault model can explain the observation at DART 51426 but not at 51425. As for the Chile tsunami, the simulated sea levels at DART 32412 and 51406 show good reproduction of the results by Yoshimoto et al. (2016) and fit the observation well except for somewhat attenuated amplitudes.

Although we successfully reproduced the simulation results of the previous works using the respective fault models at the DART stations, the simulated sea levels at SOC8 in the TIARES area still show obvious discrepancies both in amplitude and phase from the observation as indicated in Fig. 6. To explain the first peak of the observation, combinations of amplitude gain and time shift were calculated: In the Samoa tsunami event, the simulated sea level was divided by 2.65 and delayed by 99s. As for the Chile tsunami, the simulated result was divided by 1.04 and delayed by 171s. After that modification, the discrepancies of the simulation results were significantly reduced as illustrated in Fig. 6. It is noteworthy that the same modification can be applied to the simulated magnetic field, because the examination of the 2-D analytical solution by Minami et al. (2021) reveals that there is nearly a linear relationship in the amplitude of tsunami sea level change and magnetic field.

4.2 Simulation of the tsunami magnetic field

The tsunami magnetic field at SOC8 was simulated by the 3-D time-domain simulation code by Minami et al. (2017). It can calculate the tsunami magnetic field from the given velocity field using the finite element method based on the Maxwell equations. The code can support various sea water conductivities and bathymetries as well.

In the simulation of the tsunami magnetic field, the horizontal tsunami velocity by JAGURS was used, while the vertical velocity component was calculated from the simulated V_x, V_y and sea level change using the mass conservation law (Minami et al., 2017). The 3-component tsunami magnetic field with a 10s time step in the TIARES area (152ºW - 140ºW, 15ºS - 25ºS) was calculated as summarized in Table S2 in Supporting Information.

For the convenience of the initial rise examination, the horizontal components, B_x and B_y, of the simulated magnetic field were rotated to the direction of the tsunami propagation in order to compute B_h. For analyses of the phase lead of tsunami B_z and the initial rise in tsunami B_h, we compared the simulated magnetic field with that of the sea level change at SOC8 as shown in Fig. 7.
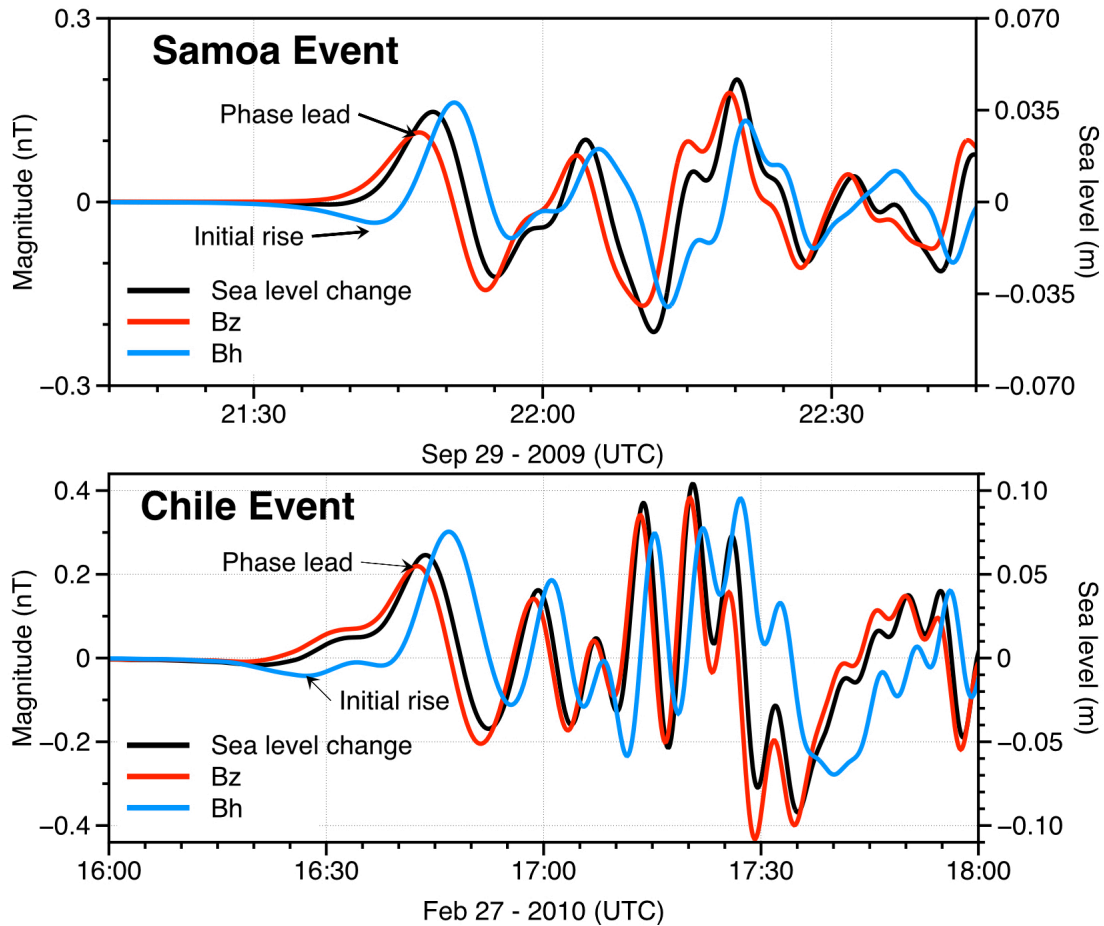
Figure 7. Comparison of the simulated sea level change with the simulated tsunami magnetic components at SOC8. The sea level change was calculated by JAGURS and tsunami magnetic components were calculated by the 3-D time-domain simulation code by Minami et al. (2017). The tsunami Bh is parallel to the direction of each tsunami propagation and was computed using the simulated Bx and By. A phase lead of tsunami Bz with respect to the sea level change and an initial rise (actually 'retreat' in this case) in tsunami Bh are clearly seen.

As shown by the comparison of tsunami Bh with respect to the tsunami sea level in Fig. 7, the initial rise (actually 'retreat' in this case) apparently appeared in both simulations. In the simulation of the 2009 Samoa tsunami, a negative peak before any peaks of sea level change is the tsunami initial rise, which is in harmony with that reported by Minami et al. (2015). The initial rise in tsunami Bh is about -0.03 nT , which corresponds to the following 3.4cm-high tsunami. However, the observed tsunami wave height at the first arrival is 1.3cm as shown in Fig. 3 upper panel, so that this simulated amplitude of initial rise must be larger than the actual amplitude.

The initial rise in Chile tsunami Bh was simulated as small as -0.04 nT. In contrast to the tsunami first arrival consisting of a single peak in the 2009 Samoa tsunami, the first arrival of 2010 Chile tsunami is more complex to have a small dual peak before the larger peak (see the lower left panel of Fig. 6). That simulated value of -0.04 nT should be similar to the actual amplitude of the initial rise, because we succeeded in reproducing the observed tsunami wave
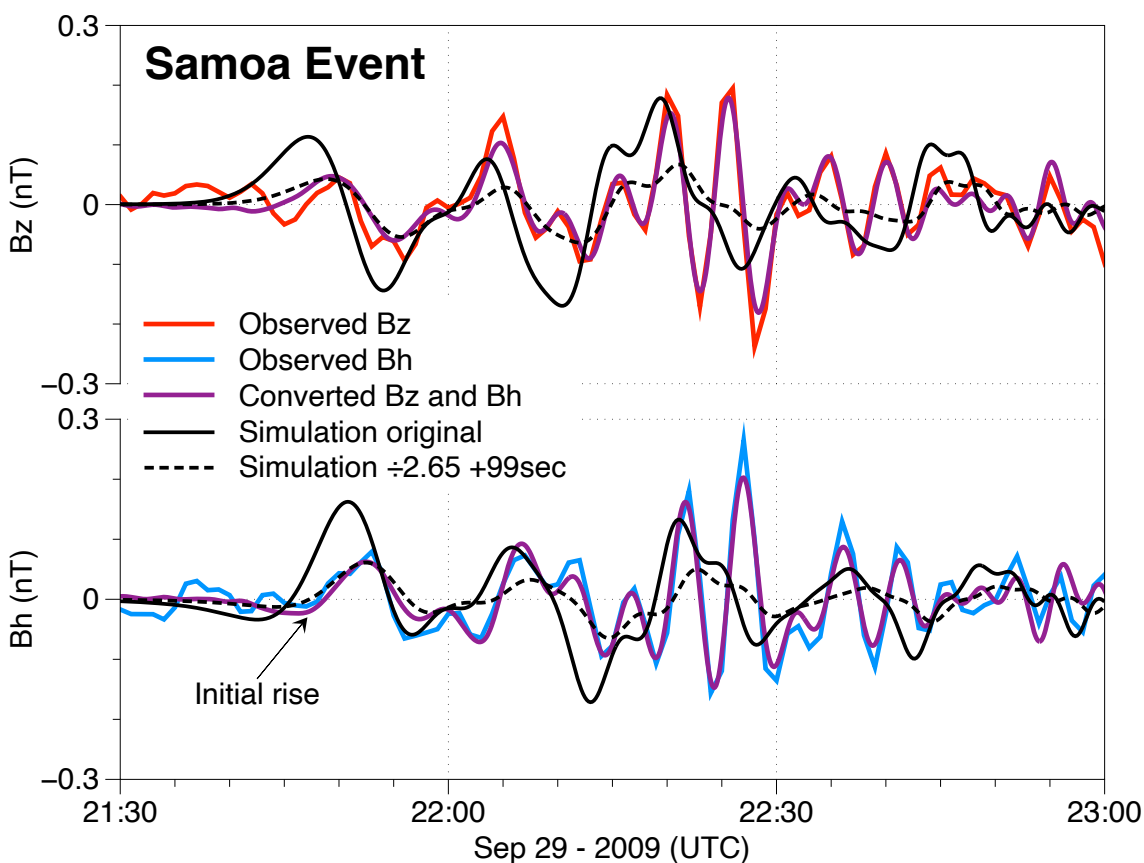
height by simulation (see Fig. 6). Although the amplitude in the Chile event was larger than that in the Samoa event, the initial rise is still hard to recognize, because the Chile event started with a small dual bump that makes it difficult to isolate the initial rise.

The phase lead of tsunami Bz, however, is still clearly seen in the simulated Bz for both events. The tsunami Bz has a small but evident phase lead with respect to the tsunami sea level change. The identified phase leads of Bz corresponding to the first peak of the tsunami wave height are indicated by arrows in Fig. 7.

In the simulation results, the initial rise may exist in both Bh of the 2009 Samoa and 2010 Chile tsunamis, although that of the latter is less prominent due to the complexity of its first arrival. Our simulation results suggest that the initial rise is a little bit too small for the Samoa tsunami and too complicated for the Chile tsunami to recognize in the observation data. We will further argue this issue in the next section by direct comparison of the simulation with the observation.

4.3 Comparison of the simulated tsunami magnetic field with the observation

In Fig. 8, the simulated magnetic fields without and with modification at SOC8 are compared with the observation as well as the magnetic field converted from the observed sea level change using the 2-D analytical solution (Minami et al., 2021).
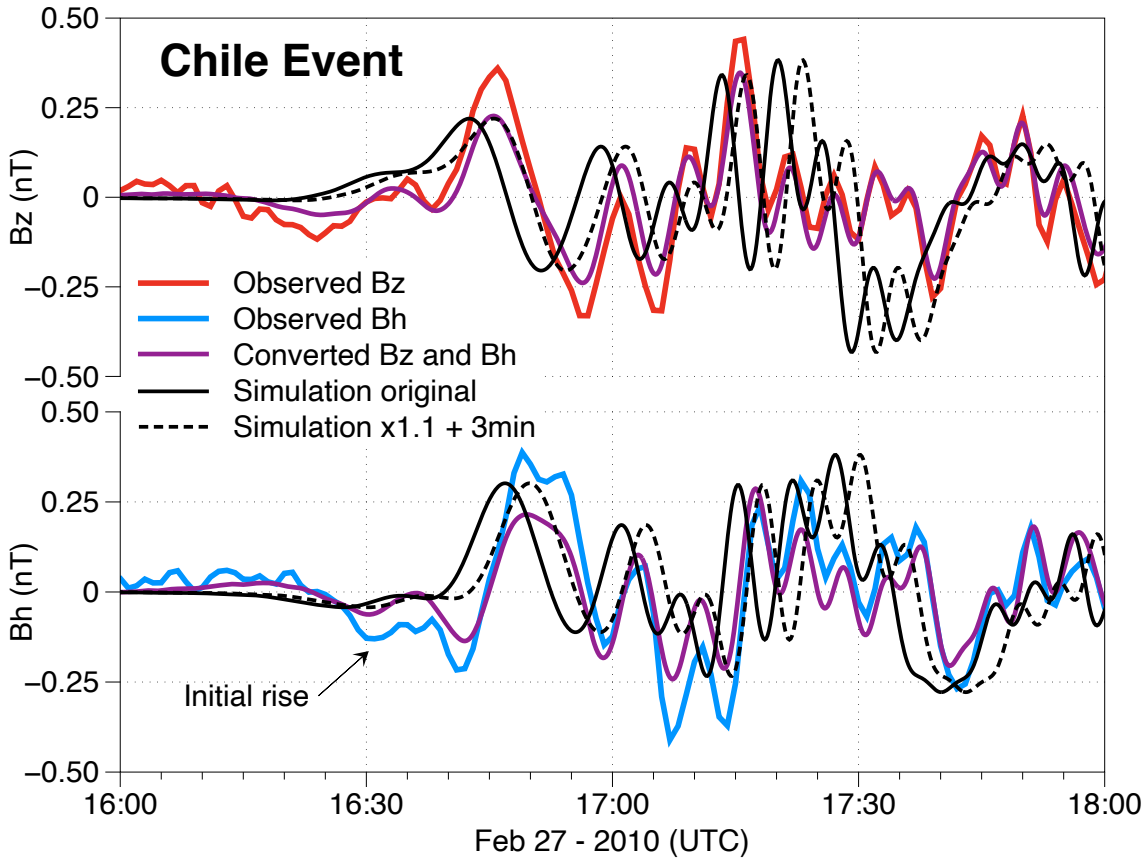
Figure 8. Comparison of the observed, simulated and converted tsunami magnetic fields for the 2009 Samoa (upper) and 2010 Chile (lower) events at SOC8. As described in Section 3, the observed data have passed through band-pass filters and the external field has been subtracted out. The converted magnetic field was calculated from the observed sea level change. The dashed lines show modification of the original simulation results by the same combination of amplitude gain and time shift per event as the sea level change. The modified simulation results have better fits to the observation and the converted results for both amplitude and arrival time.
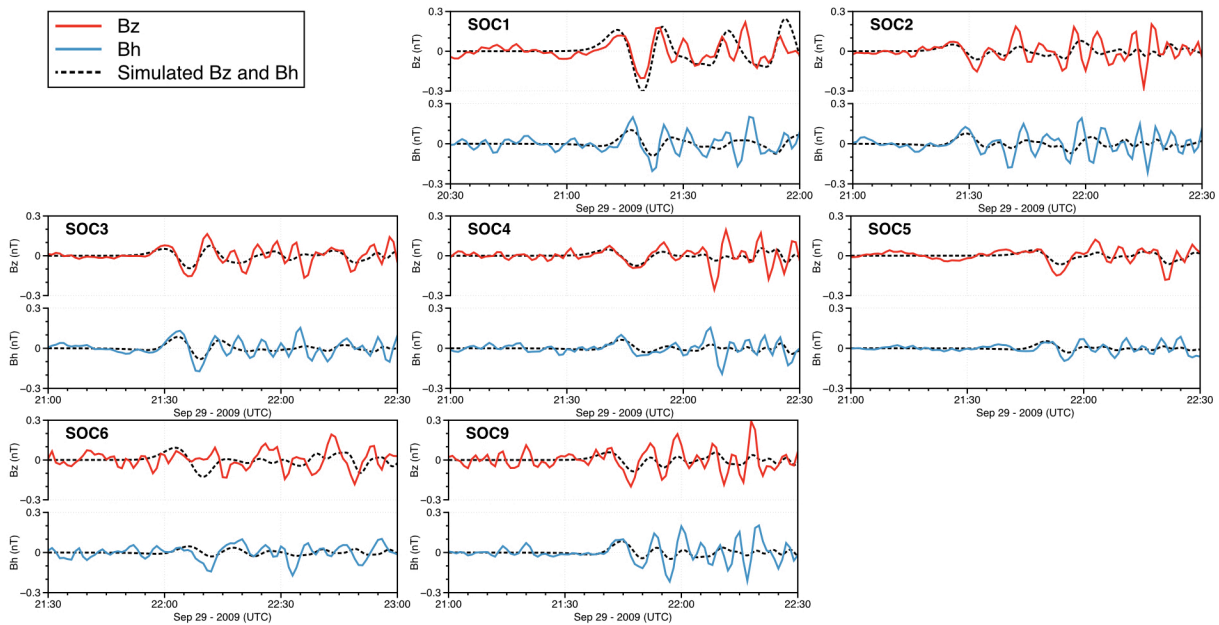
Comparison of the simulated magnetic field (black solid lines) and observation (red and blue solid lines) shows poor agreement of the simulation with the observation. The phase and amplitude discrepancies between simulation and observation are notable, similar to that between the simulated and observed sea level change shown in Fig. 6. As mentioned before, the simulated tsunami sea level change can be modified by a combination of amplitude gain and time shift to match the observation better. These results suggest that the discrepancy between the simulated magnetic field with the observation is mainly due to the inaccuracy in the tsunami velocity field simulation because the accuracy of the tsunami magnetic calculation was examined intensively (see Fig. 3 and Table 1 of Minami et al., 2017). In other word, we need a better velocity field to improve the tsunami magnetic simulation significantly.

By inspection of the modified simulation, the initial rise in Bh for both events may be present. However, the actual initial rise in the Samoa event can be as small as -0.012 nT that is

smaller than the background noise. On the other hand, in the Chile tsunami we can confirm the initial rise in observed Bh (indicated by arrow in Fig. 8). However, the initial rise in the observation, in turn, is much larger than the simulation. Compared with the converted Bz, it may be because the simulation could not fit the amplitude of the small dual peak.

From the comparison of modified simulation with the converted Bz and Bh, it can be seen that the simulation agrees with the converted magnetic field fairly well. The first arrival of simulation has moderate agreement with the converted results in the amplitude and phase in Samoa event. Also, the simulated Bz of the Chile tsunami fits the converted Bz well. It means that the simulation results were in line with the 2-D analytical solution at least for the Samoa tsunami.

Finally, we compared the modified magnetic simulation with the observation at the remaining SOC sites (SOC1~6, 9) for both events in Fig. 9. It can be seen that the modified simulation seems to fit the observation well. Also, in 2009 Samoa tsunami, a small initial rise may present in the observation of SOC2 and 3, while other SOC sites do not show such signatures. As for the 2010 Chile tsunami, the initial rises are too complicated to identify. In general, it is difficult to separate the initial rise of a tsunami preceded by a complex peak.
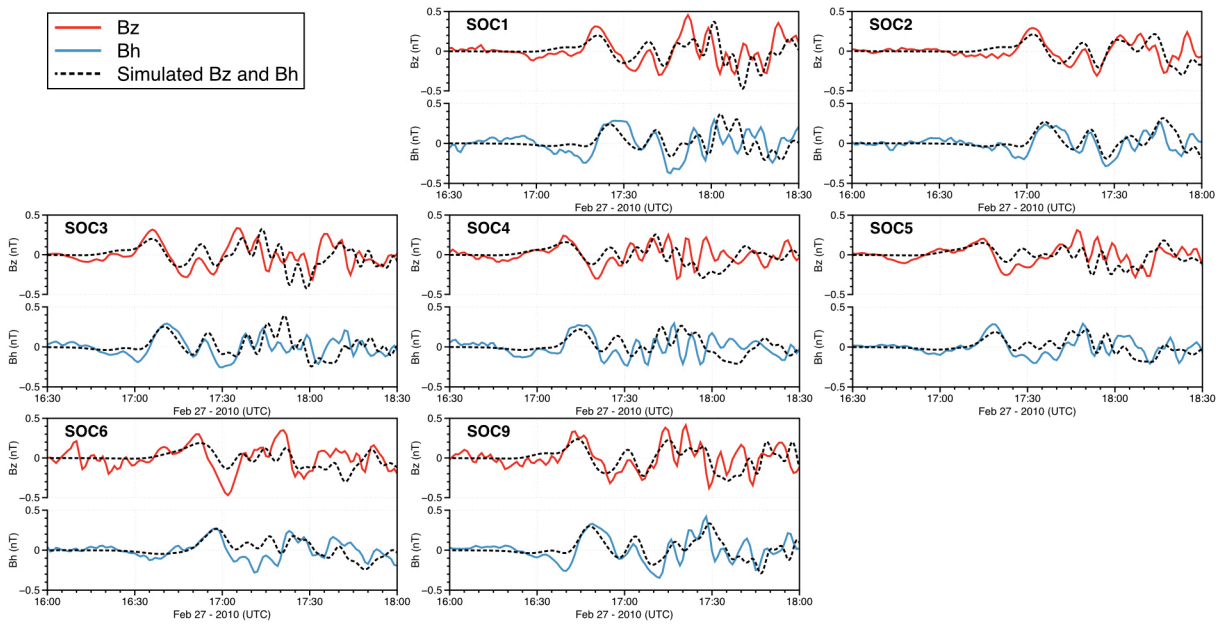
Figure 9. Comparison of simulation and observation for the tsunami magnetic field at SOC1~6, 9 at the time of the 2009 Samoa tsunami (upper) and the 2010 Chile tsunami (lower). The observed tsunami magnetic field have passed through the 3~30-minute and 3~45-minute band-pass filter for the Samoa and Chile tsunamis respectively, and the external field has been subtracted. Also, the simulated tsunami magnetic field have divided by 2.65 and delayed by 99s for the Samoa tsunami, and divided by 2.65 and delayed by 99s for the Chile tsunami.

5 Discussion and Conclusion

Presence of the phase lead in tsunami Bz and the initial rise in Bh has been shown by the simulation in previous studies. However, few have been confirmed by the observation so far. In this study, we examined the phase lead of tsunami Bz as well as the initial rise in tsunami Bh using the combination of observation and simulation of both tsunami sea level change and magnetic field at the times of the 2009 Samoa and 2010 Chile earthquakes using the TIARES dataset.

First, the tsunami signals were successfully extracted from the observed ocean bottom pressure changes and magnetic fields of both 2009 Samoa and 2010 Chile tsunamis in spite of the very large epicentral distances. The phase of tsunami Bz always has phase leads of 90º with respect to Bh, which is in line with the observation of other tsunami events (Toh et al., 2011, Minami et al., 2017). Also, the converted sea level changes using the observed tsunami magnetic field are agree with the observed sea level change very well. It is evident that the tsunami magnetic signals on the seafloor were identified clearly at each SOC station, even though the amplitudes of tsunami magnetic field were small, 0.2 nT and 0.3 nT for the 2009 Samoa and 2010 Chile tsunamis, respectively.

The phase lead of tsunami Bz and the initial rise of tsunami Bh were studied using the unique simultaneous observation of both ocean bottom pressure and magnetic field. Based on the comparison of the observed sea level change with the observed magnetic field, we confirmed that tsunami Bz has its phase lead with respect to the sea level change, which is in line with the

prediction by Minami et al. (2015). This means that we may be able to exploit the significant phase lead of tsunami Bz for the purpose of the tsunami early warning. We also showed that the phase lead of tsunami Bz w.r.t. the sea level change in each main frequency components are in harmony with the leading time of each component using the analytical solution described in Minami et al. (2021). Our results indicated that the value of the phase lead is almost identical over the tsunami period band, while the leading time gets larger linearly against the tsunami periods. It is noteworthy that this study investigated the tsunami magnetic field in the averaged 4800m water depth, which is classified as "Self-induction dominant case" and "Intermediate case" according to Minami et al. (2015). On the other hand, the behavior of tsunami magnetic field in shallow water, named "diffusion dominant case" in Minami et al. (2015), is still not confirmed and needs more investigation.

On the other hand, the initial rise in the tsunami Bh was not detected clearly in the observation of both tsunami events. In the 2009 Samoa tsunami, the very first wave of tsunami was too small to detect an observable initial rise in Bh, although our 3-D time domain magnetic simulation predicted its presence. As for the 2010 Chile tsunami, we probably captured the initial rise because a small 'retreat' in Bh is recognizable. However, the first wave of the 2010 Chile tsunami was rather complicated to identify the initial rise clearly using the first arrival. These results suggest that further study on the initial rise in tsunami Bh is necessary in order to apply it to tsunami early warning.

Precision of the conversion equations of tsunami magnetic field to sea level change (and vice versa) by Minami et al. (2021) was also verified using the simultaneous data of different physical quantities. Comparison of the observed and converted sea level changes indicates that the equations can precisely predict the tsunami sea level change based on the known tsunami Bz or Bh (and vice versa), provided that the ocean depth as well as the sub-seafloor electrical structure is known. It also implies that the tsunami magnetic field is equivalent to the tsunami sea level change and useful in tsunami research such as the earthquake fault model inversion, since the tsunami Bz and Bh are proved to be very good proxies of the sea level change by this study. We created a dataset of sea level changes converted from the observed tsunami magnetic field in the TIARES area (see Data Availability Statement). However, there still exists discrepancy between the converted and observed magnetic field in the 2010 Chile tsunami due mainly to the 3-D effect of the tsunami in concern.

Using the 3-D tsunami magnetic field simulations in time domain including the tsunami velocity field simulation, the presence of initial rise and the 3-D effect were investigated in the magnetic field of both tsunami events. The tsunami velocity fields were calculated from the fault model of Firtz et al. (2011) and Yoshimoto et al. (2016) for Samoa and Chile, respectively. Comparison of the simulated and observed tsunami sea level change indicated that simulated velocities based on the given source models have too large amplitudes around the TIARES area to explain the observed tsunami magnetic fields. Very good fits of the observed magnetic signal to the converted magnetic signal described in Section 3 encouraged us to calculate the best-fit magnetic time-series to the observation from the simulated time-series by changing two parameters, i.e., the amplitude gain and the time shift. The results show that the major source of simulation error consists in the inaccurate velocity simulation, which may also explain the reason for the discrepancy between the simulated magnetic field and the observation in previous studies (Zhang et al., 2014; Minami et al., 2017). Better source fault models using the converted tsunami sea level change in the TIARES area are definitely in need here. Further studies in search for the

best tsunami simulation such as more precise dispersion calculation, better earthquake source models are essential to explain the TIARES observation, which is, unfortunately, beyond the scope of the present paper.

The 3-D effects of both tsunamis were studied by our 3-D magnetic field simulation as well. The converted sea level change fit the observation well for the Samoa event, while the converted amplitude is significantly smaller than the observation for the Chile event. It means that the 3-D effect is not very large in the case of the 2009 Samoa tsunami but may be significant in the 2010 Chile tsunami. It should be noted that our velocity simulation is 2-D in the sense that JAGURS outputs horizontal velocity components alone. According to Minami et al. (2021), the vertical velocity component may be able to produce small Bz (and Bh) even in the equatorial region, which happens only when the tsunami propagates largely in a direction parallel to the horizontal component of the geomagnetic main field. However, both tsunami events treated here are mainly traveled in the east-west direction, which is perpendicular to the direction of the background geomagnetic main field around the TIARES area. It, therefore, is unlikely that contribution of the vertical velocity component amends results of this paper drastically. In anyways, better tsunami source models are still in need for achieving better fits to the observed tsunami magnetic fields.

Data Availability Statement

The observed data of magnetic field and pressure in the TIARES area used in this study was provided by the TIARES experiment (Suetsugu et al., 2012). The magnetic field data at PPT station on Tahiti Island can be download in the Word Data Center for Geomagnetism, Kyoto (http://wdc.kugi.kyoto-u.ac.jp/catmap/obs.html). The observed tsunami sea level change and magnetic field which extracted from the TIARES data can be accessed from (https://doi.org/10.5281/zenodo.5111644). In terms of the simulation of the 2009 Samoa and 2010 Chile tsunamis, the source models of these earthquakes are the 'Mega 1' fault model of Fritz et al. (2011) and the 'all DART only' fault model of Yoshimoto et al. (2016), respectively. JAGURS, the tsunami velocity field simulation software used in this study are available from Baba et al., (2017). The time-domain tsunami magnetic field simulation code used in this study was provided by Minami et al., (2017). The simulated tsunami sea level change and magnetic field of these two events which shown in this paper can be accessed from (https://doi.org/10.5281/zenodo.5111644). In addition, we provide a dataset of sea level changes converted from the observed tsunami magnetic field in the TIARES area in the Zenodo repository (https://doi.org/10.5281/zenodo.5111644).

Acknowledgments

References

Araki, E. and Sugioka, H. (2009), Calibration of deep-sea differential pressure gauge. *JAMSTEC Report of Research and Development 2009*, 141-148. https://doi.org/10.5918/jamstecr.2009.141

Baba, T., S. Allgeyer, J. Hossen, P.R. Cummins, H. Tsushima, K. Imai, K. Yamashita, and T. Kato. (2017), Accurate numerical simulation of the far-field tsunami caused by the 2011 Tohoku earthquake, including the effects of Boussinesq dispersion, seawater density stratification, elastic loading, and gravitational potential change (Version 5.2). *Ocean Modelling*, 111, 46-54. https://doi.org/10.1016/j.ocemod.2017.01.002

Bernard, E. & Meinig, Christian. (2011). History and future of deep-ocean tsunami measurements. *OCEANS'11 - MTS/IEEE Kona, Program Book*, 1-7. https://doi.org/10.23919/OCEANS.2011.6106894

Fritz, H.M., Borrero, J.C., Synolakis, C.E., Okal, E.A., Weiss, R., Titov, V.V., Jaffe, B.E., Foteinis, S., Lynett, P.J., Chan, I.C. and Liu, P.L.F. (2011), Insights on the 2009 South Pacific tsunami in Samoa and Tonga from field surveys and numerical simulations. *Earth-Science Reviews*, 107(1-2), 66-75. https://doi.org/10.1016/j.earscirev.2011.03.004

Kawashima, I. & Toh, H. (2016) Tsunami-generated magnetic fields may constrain focal mechanisms of earthquakes. *Scientific Reports*, 6, 28603. https://doi.org/10.1038/srep28603

Matzka, J., Stolle, C., Yamazaki, Y., Bronkalla, O., & Morschhauser, A. (2021). The geomagnetic Kp index and derived indices of geomagnetic activity. *Space Weather*, 19, e2020SW002641. https://doi.org/10.1029/2020SW002641

Minami, T., and Toh, H. (2013), Two-dimensional simulations of the tsunami dynamo effect using the finite element method. *Geophysical Research Letters*, 40, 4560– 4564. https://doi.org/10.1002/grl.50823

Minami, T., H. Toh, and R. H. Tyler. (2015), Properties of electromagnetic fields generated by tsunami first arrivals: Classification based on the ocean depth. *Geophysical Research Letters*, 42, 2171–2178. https://doi.org/10.1002/2015GL063055

Minami, T., Toh, H., Ichihara, H., & Kawashima, I. (2017), Three-dimensional time domain simulation of tsunami-generated electromagnetic fields: Application to the 2011 Tohoku earthquake tsunami (Version 1.1). *Journal of Geophysical Research: Solid Earth*, 122, 9559– 9579. https://doi.org/10.1002/2017JB014839

Minami, T., Schnepf, N.R. & Toh, H. (2021), Tsunami-generated magnetic fields have primary and secondary arrivals like seismic waves. *Scientific Reports*, 11, 2287. https://doi.org/10.1038/s41598-021-81820-5

Schnepf, N.R., Manoj, C., An, C. et al. (2016), Time–frequency characteristics of tsunami magnetic signals from four Pacific Ocean events. *Pure and Applied Geophysics*, 173, 3935– 3953. https://doi.org/10.1007/s00024-016-1345-5

Suetsugu, D., Shiobara, H., Sugioka, H. et al. (2012), TIARES Project—Tomographic investigation by seafloor array experiment for the Society hotspot. *Earth, Planets and Space*, 64, i–iv. https://doi.org/10.5047/eps.2011.11.002

Sugioka, H., Hamano, Y., Baba, K. et al. (2014), Tsunami: Ocean dynamo generator. *Scientific Reports*, 4, 3596. https://doi.org/10.1038/srep03596

Toh, H., Satake, K., Hamano, Y., Fujii, Y., and Goto, T. (2011), Tsunami signals from the 2006 and 2007 Kuril earthquakes detected at a seafloor geomagnetic observatory. *Journal of Geophysical Research*, 116, B02104, https://doi.org/10.1029/2010JB007873

Tozer, B, Sandwell, D. T., Smith, W. H. F., Olson, C., Beale, J. R., & Wessel, P. (2019), Global bathymetry and topography at 15 arc sec: SRTM15+. *Earth and Space Science*, 6, 1847–1864. https://doi.org/10.1029/2019EA000658

Tyler, R. H. (2005), A simple formula for estimating the magnetic fields generated by tsunami flow. *Geophysical Research Letters*, 32, L09608, https://doi.org/10.1029/2005GL022429

Wessel, P., Luis, J. F., Uieda, L., Scharroo, R., Wobbe, F., Smith, W. H. F., & Tian, D. (2019), The Generic Mapping Tools version 6. *Geochemistry, Geophysics, Geosystems*, 20, 5556–5564. https://doi.org/10.1029/2019GC008515

Yoshimoto, M., Watada, S., Fujii, Y., and Satake, K. (2016), Source estimate and tsunami forecast from far-field deep-ocean tsunami waveforms—The 27 February 2010 Mw 8.8 Maule earthquake. *Geophysical Research Letters*, 43, 659–665. https://doi.org/10.1002/2015GL067181

Zhang, L., Utada, H., Shimizu, H., Baba, K., and Maeda, T. (2014), Three-dimensional simulation of the electromagnetic fields induced by the 2011 Tohoku tsunami. *Journal of Geophysical Research: Solid Earth*, 119, 150– 168. https://doi.org/10.1002/2013JB010264

Supporting Information References

Chave, A. and Thomson, D. (2003), A bounded influence regression estimator based on the statistics of the hat matrix. *Journal of the Royal Statistical Society Series C* 52. 307-322. https://doi.org/10.1111/1467-9876.00406

Matsumoto, K., Takanezawa, T. and Ooe, M. (2000), Ocean tide models developed by assimilating TOPEX/POSEIDON altimeter data into hydrodynamical model: A global model and a regional model around Japan. *Journal of Oceanography* 56, 567–581. https://doi.org/10.1023/A:1011157212596

Thébault, E., Finlay, C.C., Alken, P. et al. (2015), Evaluation of candidate geomagnetic field models for IGRF-12. *Earth Planet Sp* 67, 112. https://doi.org/10.1186/s40623-015-0273-4

Tyler, R.H., Boyer, T.P., Minami, T. et al. (2017), Electrical conductivity of the global ocean. *Earth Planets Space* 69, 156. https://doi.org/10.1186/s40623-017-0739-7